# Conductance of a phenylene-vinylene molecular wire: Contact gap and tilt angle dependence

A. Bilić,[1, *] ZC,[2] BG,[3] J. D. Gale,[4] and S. Sanvito[5]

[1]*CSIRO Mathematical and Information Sciences,*
*Private Bag 33, Clayton South 3169 VIC, Australia*

[2]*XXX*

[3]*YYY*

[4]*Nanochemistry Research Institute, Department of Chemistry,*
*Curtin University of Technology, P.O. Box U1987, Perth 6845, Western Australia*

[5]*School of Physics and CRANN, Trinity College, Dublin, Ireland*

(Dated: November 9, 2009)

# Abstract

Charge transport through a molecular junction comprising an oligomer of $p$-phenylene-vinylene between gold contacts has been investigated using density functional theory and the non-equilibrium Green's function method. The influence of the contact gap geometry on the transport has been studied for elongated and contracted gaps, as well as various molecular conformations. The calculated current-voltage characteristics show an unusual increase in the low bias conductance with the contact separation. In contrast, for compressed junctions the conductance displays only a very weak dependence on both the separation and related molecular conformation. However if the contraction of the gap between the electrodes is accommodated by tilting the molecule, the conductance will increase with the tilting angle, in line with experimental observations. It is demonstrated that the effect of tilting on transport can be interpreted in a similar way to the case of the stretching the junction with an upright wire. The lowest conductance was observed for the equilibrium gap geometry. With the dominant transport contribution arising from the $\pi$-system of the frontier junction orbitals, all the predicted increases in the conductance arise simply from the better band alignment between relevant frontier orbitals at the non-equilibrium geometries at the expense of weaker coupling with the contacts. Finally, based on present findings, the operating physical principles of a device based on an oligo-phenylene-vinylene wire are proposed.

---

$^{*}$Corresponding author. E-mail: ante.bilic@csiro.au

# I. INTRODUCTION

Over the past decade greater interest has arisen in molecular electronics, a rapidly growing field that is a prospective successor to metal-oxide-semiconductor based electronics (for a recent review see ref. [1] and references therein). Electron transport through molecular junctions has been exploited to fabricate two- and three-terminal devices, such as rectifiers, memory switches, and transistors. However, there remain many challenges to this promising technology, such as device stability, reproducibility, and control over the transport. Oligomers of $p$-phenylene-vinylene provide a promising platform for the fabrication of high conductivity molecular devices. The structural motif of oligo-$p$-phenylene-vinylene (OPV) consists of coplanar phenyl moieties connected by vinylene links, which provide the conformational rigidity through a high rotational barrier and, at the same time, extend the conjugation of the system. Owing to these properties phenylene-vinylene polymers are frequently used in the synthesis of organic semiconductor devices [2]. Recently, thiol-capped OPV derivatives deposited between metal electrodes have been exploited for the fabrication of two- and three-terminal devices [3–6]. In parallel to the experimental studies, significant progress has been made in the modelling of molecular junctions, although quantitative agreement between theory and experiments has remained elusive [7, 8].

The present computational work reports on the dependence of the conductance of a molecular junction comprising a thiol-capped OPV derivative with 3-rings (OPV3) between gold contacts as a function of the contact gap separation. Symmetric elongation and contraction of the junction away from the equilibrium spacing have been studied. In addition, the effects of the molecular tilting are investigated. For the sake of simplicity, extensive reconstructions of the gold contact surfaces [9–11] are not considered here. We find a general

trend of enhanced conductance as the geometry deviates from the upright orientation of the molecular wire in the optimal contact gap. This effect invariably arises because of the reduced coupling strength at the contacts, which results in the more favorable alignment of the relevant frontier orbitals with the electrodes Fermi level. For an elongated junction a highly conductive state of the wire is predicted by a substantial separation from the leads, with a linear I-V characteristic over a useful bias voltage range, and a prospect for both transistor and switching operation. For the compressed junctions with a distorted OPV3 wire little variation of conductance is found, owing to the resilience of the conjugated frontier molecular orbitals. However, when OPV3 is tilted a similar I-V curve to that of the elongated junctions is predicted, again because of the better band line-up arising through the reduced bonding at the interface. The latter findings, while in agreement with recent experimental observations of Haiss *et al* [12, 13], offer a different interpretation of their results for related wires.

## II. COMPUTATIONAL METHODOLOGY

Geometry optimizations were conducted using DFT as implemented in the SIESTA program [14, 15]. In the SIESTA methodology a linear combination of atomic orbitals (LCAO) is used to expand the Kohn-Sham eigenstates. Core electrons and nuclei are replaced by norm-conserving pseudopotentials in a fully separable form [16]. The modified scheme of Troullier and Martins [17] was exploited to generate pseudopotentials for Au, C, H, and S, with relativistic corrections included for Au, C, and S. For the exchange and correlation potential the PBE functional [18], a form of generalized gradient approximation (GGA), was used for both pseudopotential generation and in the actual calculations. The one-electron Kohn-Sham eigenstates were expanded in a basis of strictly localized [19] numerical pseudo atomic orbitals [20]. Basis functions were obtained by finding the eigenfunctions of the isolated atoms confined within a sphere. The range of the atomic orbitals was chosen so as to obtain an energy increase of 7 mRy arising due to the spherical confinement. This results in orbital confinement radii of 2.38–3.07 and 3.74 Å for the molecule and gold orbitals, respectively. For transport calculations smaller energy shifts have been recommended [21, 22], but because of the rather limited surface area of the supercell (see below), the tighter confinement of the orbitals is favorable, to minimize the overlap of periodic images of the molecule. Thus, even in the case of the most distorted geometry considered here, for which the minimal distance between two atoms placed in different periodic replica was 5.57 Å, the orbital overlap was still rather insignificant. A split-valence scheme was employed to generate a single-$\zeta$ basis set for the $6s$ and $5d$ states of Au, and a double-$\zeta$ basis set for the $1s$ state of H, $2s$ and $2p$ states of C, $3s$ and $3p$ states of S, with a single-$\zeta$ shell of polarization functions for all four elements. SIESTA uses an auxiliary real space mesh to evaluate terms based

on charge density and an equivalent plane-wave cutoff of 350 Ry was used to determine the mesh spacing. All the atomic geometries were relaxed via conjugate gradient optimization until the forces were smaller 10 meV $\text{Å}^{-1}$. While SIESTA supports spin-polarized treatment of electrons, to reduce the computational cost only unpolarized calculations (i.e. restricted open shell in the case of the de-hydrogenated OPV3 biradical) have been employed in the present work.

The optimized geometries from the SIESTA computations, as well as all the relevant computational parameters, were subsequently employed in electron transport calculations. The latter were conducted using the non-equilibrium Green's function (NEGF) approach as implemented in the SMEAGOL package [23–25], which is interfaced to SIESTA.

The two-terminal device was modeled using a supercell geometry of the Au(111) surface consisting of several atomic layers and a vacuum gap in which the OPV3 molecule was placed. The application of periodic boundary conditions along all the three Cartesian directions yields an infinite array of periodically repeated slabs separated by regions of vacuum. The gold slab was 10 atomic layers thick, and the boundaries of the supercell were set up so that the single slab forms the two contacts, with 5 Au atomic layers on each side. The system was then partitioned into two leads and a scattering region. The three layers of Au at the bottom and top of the cell (i.e., the inner six layers of the slab) were the leads and their geometries were fixed to the bulk positions. The two Au layers below and above the vacuum region (i.e., the outer two layers on each side of the slab) were taken as parts of the extended molecule, with which they form the scattering region (this is the part treated at the NEGF self-consistent level). The geometry of the extended molecule was always optimized prior to the transport calculation. The thickness of vacuum, i.e. the separation of the electrodes varied from 19.57 to 28.57 Å. A single OPV3 molecule was inserted in the middle of the

vacuum region, with S atoms approximately above the three-fold hollow sites. However, because of the A-B-C stacking sequence of atomic layers on the gold (111) surface, the two faces of the slabs are not fully symmetric. Thus, if the S binding site on one of the contacts is FCC hollow, its counterpart on the opposite contact is HCP hollow. Consequently, the coupling at the thiolate-gold interface will be somewhat stronger for the former site [26].

A (3×3) superstructure was employed for the Au(111) surface resulting in nine gold atoms per layer. This represents a moderate 1/9 OPV3 monolayer coverage, which guarantees that the molecules in neighboring cells are sufficiently separated (i.e., non-interacting) [26–33]. For the geometry optimizations, as well as for the transport computations, the Brillouin zone integrations were performed on a 3×3 k-point Monkhorst-Pack mesh in the plane of the surface. For the calculation of the bulk electronic structure of the gold leads the reciprocal space was sampled on a 3×3×100 grid, with the denser sampling in the direction of transport. Finally, for the optimizations of the gas phase OPV3 in a large supercell only the $\Gamma$-point was used. In the transport calculations the complex part of the integral leading to the charge density is computed by using 25 energy points on the complex semi-circle, 20 points along the line parallel to the real axis and 9 poles. The integral over real energies necessary at finite bias is evaluated over at least 500 points [23, 24].

The lattice parameter of gold was obtained from bulk computations of total energy versus the size of the unit cell. While this property is needed as an input parameter to the subsequent supercell computations, calculations of this type are also useful as they provide indication of the accuracy of the computational approach. The Brillouin zone integration was performed on a Monkhorst-Pack 8×8×8 k-point mesh. The fit to an equation of state gives a lattice constant of 4.196 Å and a bulk modulus of 141 GPa. These values are in an acceptable agreement with those from experiments, 4.08 Å and 170 GPa, and in excellent

agreement with those evaluated with the PW91 functional by using an almost complete plane wave basis set, 4.2 Å and 150 GPa [27]. The band structure of gold evaluated with the single-$\zeta$ plus polarization function (SZP) basis set also shows remarkable similarity with that from the plane wave approach. The results from these simple tests thus justify the use of the modest SZP basis set for Au.

OPV3 without thiol ends, better known as 1,4-distyrylbenzene, can take two conformations illustrated in Fig. 1, *trans,cis* and *trans,trans*. Because of the limited surface area of the supercell and narrower profile of the former conformation, most calculations employed this geometry. However, for the equilibrium contact separation, we have verified that the differences between the conductance of the wire in the two conformations are negligible. Therefore the *trans,trans* conformation was not further considered in the present study.

## III.  RESULTS AND DISCUSSION

### A.  Wire elongation

The equilibrium separation for the junction was estimated from the length of the OPV3 molecule in the gas phase and previously calculated distances between sulfur and gold atoms on the surface for phenylthiol [26]. It is commonly assumed that thiols adsorb on gold dissociatively, i.e. by breaking the S-H bond, although both chemisorbed and physisorbed species can be observed at equilibrium [34]. Since dissociation is the dominant mechanism, we have considered the gas phase OPV3 in the de-hydrogenated biradical form. The optimized S-S distance was 19.63 Å for the *trans,cis* conformation. Assuming a distance of 2.52 Å between the S and the Au atoms over the FCC hollow site of the lower surface and 2.56 Å over the HCP site at the opposite, upper face, the equilibrium contact distance is set to 23.07 Å for the OPV3 in the upright orientation. A subsequent optimization of the extended molecule did not cause any notable change in the geometry. The calculated I-V characteristics are shown in the upper panel of Fig. 2. It is interesting to compare it with the one previously reported for OPV3 [35], also shown in the upper panel of Fig. 2. Despite the qualitative agreement, the discrepancies between the two are clear: the previously published curve predicts a higher conductance for low bias and it saturates earlier. For high biases the two are in rather good agreement. It is not clear what are the reasons behind these discrepancies. A very similar geometry of the supercell was used in both studies. The previous study utilized LDA calculations, and, consequently the S-Au distance was slightly shorter, but the report suggested that no qualitative difference when the distance was increased to match that obtained at the GGA level, or even when a GGA functional was employed [35]. The most plausible explanation is that the combination of different pseudopotentials, basis sets,

9

and exchange-correlation flavors utilized in the two studies gives rise to the differences in the I-V curve.

From the equilibrium separation, the contact distance was then gradually increased in steps of 0.5 Å. For each step the molecule was placed in the gap center, equally apart from both contacts, and optimized. This is a different approach to junction stretching from those commonly found in the literature [9, 36, 37], where a single contact is gradually pulled away from the junction, eventually resulting in the molecule asymmetrically attached to only one of the two contacts. The latter is very similar to the experimental break junction technique [38] and the closely related $I(s)$ method [12, 13]. The $I(s)$ method involves capturing molecules between a gold scanning probe microscope tip and gold substrate and recording the current as a function of distance as the molecule is stretched until the junction is cleaved. While the symmetric bond breaking considered here does not correspond to any actual experimental technique, we believe such a geometry is more appropriate for the spin un-polarized account of electrons employed here and the biradical nature of the wire. Given the sizeable separation between the two ends, the thiolate caps can be viewed as a pair of local doublets, hence here they are treated at the symmetric footing. A more profound reason for this setup was to avoid the situation where the molecule is strongly coupled to one of the contacts and only weakly to the other contact. In the case of the asymmetrical attachment to one side of the junction the conductance gap would be associated simply with the gap between the highest occupied (HOMO) and lowest unoccupied (LUMO) molecular orbital, regardless of the actual metal contacts [39, 40]. In contrast, for the symmetric setup employed here the conductance gap is expected to be determined by the energy difference between the contact Fermi level $E_F$ and molecular orbital whose energy is closest to $E_F$ [39, 40]. Alternatively, one may think of this setup as a hypothetical device where the wire

10

is firmly gated to a third electrode, while the other two electrodes are shifted symmetrically with respect to it.

The calculated I-V characteristics for the stretched junctions are shown in the upper panel of Fig. 2. Most of the curves follow the familiar trend observed for the conjugated, thiol-capped, molecular wires between gold contacts; a slow increase in the current with the voltage for a low bias, followed by a plateau or a drop, which results in a negative differential resistance (NDR), and then a steeper increase. The I-V curves manifest a high degree of symmetry between positive and negative bias, which is expected given the rather symmetric geometry. It is interesting and counter-intuitive that for low and moderate bias voltages the junctions with wider gap separation yield higher currents and, consequently, higher associated conductances at low bias, as Table I shows. This phenomenon has already been noticed for asymmetrically stretched junctions with the prototypical phenyldithiol (PDT) molecular wire [41–43]. It arose there because the peak in the transmission spectra associated with the HOMO moved up in energy with increased contact separation, bringing it closer to the Fermi level. Thus, even though the coupling between the wire and the contacts gets weaker, it is more than compensated by the better level alignment of the relevant frontier orbitals. A similar effect is observed for the symmetrically stretched junction. In fact, for the current setup, this effect is enhanced because the favorable band alignment takes place on both ends of the wire. Eventually, the I-V characteristics exhibit the highest conductance, ca. 15 $\mu$S in the low bias regime, at the extra gap separation of 3.5 Å. It is demonstrated below that a tangible coupling to gold still persists even at this elongation. In order to verify that the high current through the elongated junction effect is not a numerical artefact, the gap was further elongated by 5.5 Å. The corresponding current (not shown) dropped by two orders of magnitude as the transmission coefficient (not shown) dropped practically to zero.

Hence, as expected, the regime of high conductivity is limited to a small range of distances between gold and sulfur.

## B. Wire compression

Similarly to the case of elongated junctions, the geometries of the compressed junctions were computed by reducing the contact distance gradually in steps of 0.5 Å. Even though this process does not correspond to any particular experimental setup, it is worth studying because it has been shown that the conductance of flexible molecular wires, as a function of the contact gap, exhibits a substantial temperature dependence [12]. This indicates the possibility of a number of molecular conformations bridging the gap, with the temperature dependence arising from the thermal distribution of conformations and their associated conductance values. The process of compression is illustrated in Fig. 3. In the first step, the geometry is only slightly bent away from that in equilibrium. However, with the following step an important conformational change takes place at the upper Au-S interface; from the HCP hollow adsorption site in the first panel, the upper S atom flips over the bridge site closer to the FCC binding site. This transformation, and subsequent steps, can be followed by looking at Fig. 4 of ref. [26], which shows a two-dimensional potential energy surface (PES) for phenylthiol on the Au(111) surface. When the gap is contracted by 1.0 Å the binding site for the S atom changes from HCP (for phenyl group in upright orientation) to a site on the minimum energy path between FCC (phenyl group in upright orientation) and bridge (the plane of the phenyl group almost parallel with the surface). Then, as the gap separation is further reduced, the S atom is expected to shift slightly back, closer to the bridge site with its phenyl ring tilted closer to the surface. This is exactly what is observed in Fig. 3. Eventually, as the gap separation is reduced by 3.5 Å, the upper S atom is adsorbed

12

vertically above the bridge site and its coordinating ring is tilted at a large angle away from the upright conformation.

The change in the nature of the S-Au bond at the upper surface over the series of compression steps is also reflected in the change of the S-S distance. As Table I shows, a gap compression of 0.5 Å results in a smaller reduction of 0.43 Å between the S ends. The difference of 0.07 Å comes from the reduction in S-Au bond lengths, indicating the attractive interaction at the interfaces. However, during the next step, in which the gap is compressed by a total of 1.0 Å, the S-S distance is reduced even more, by 1.20 Å. This shows that the molecule shrinks at the expense of the increased S-Au bond lengths, reflecting a more repulsive interaction at the interface. The interaction becomes increasingly more repulsive with every subsequent step, as the changes in the S-S distance relative to the gap contraction, shown in Table I, suggest. Interestingly, throughout this process the S atom on the lower face remains adsorbed on the FCC site and, in agreement with the previously computed PES [26], the associated phenyl ring, although tilted, remains closer to the upright orientation.

The calculated I-V characteristics for three compressed junctions are shown in the lower panel of Fig. 2. In contrast to those for the elongated junctions in the upper panel, these curves exhibit very little dispersion at low voltages. Hence, a low bias conductance of ca. 2.5 $\mu$S is obtained for all three, as reported in Table I. The curve for the 0.5 Å compressed junction deviates only marginally from that at equilibrium separation, which is expected given the similar geometry. However, even for the very distorted geometries, such as those at 2.0 and 3.5 Å reduced separations, the associated characteristics exhibit substantial variance with the equilibrium curve only at voltages in excess of 1 V.

It is clear that in a contracted junction the OPV3 wire does not need to adopt a bent conformation like the one described above, but it can remain straight if it tilts away from

13

the normal. In fact, in a typical experimental setup, such as the $I(s)$ method, involving a rigid molecular wire, the reduced distance between the contacts usually results in tilting the molecular orientations away from the surface normal [12, 13]. Two tilted conformations have been considered, at 15º and 30º away from the normal, with contact gaps reduced by 0.5 and 2.0 Å from the equilibrium, respectively, and molecular plane perpendicular to the contact surfaces. Both are illustrated in Fig. 4. The lower S atom is again located at the FCC hollow site, while the upper S atom sits at the HCP hollow and between the HCP hollow and bridge site for the 0.5 and 2.0 Å compressed junctions, respectively. Hence, the adsorption sites and, presumably, the associated electronic couplings between the molecule and the electrodes, approximately match their counterpart bent conformations of Fig. 3. However, the resulting currents, shown in the lower panel of Fig. 2, differ substantially. The tilted wires yield a better low bias conductance, as Table I shows. The characteristic of the 30º tilted OPV3 wire, in particular, exhibits a higher conductance than any other compressed molecular junction considered in the present work.

## C. Discussion

The most interesting result of the present study is the notably enhanced conductance of OPV3 with the separation from the gold contacts. A similar effect has been predicted for other molecular wires attached to gold electrodes via thiol links [8, 37, 41–43]. Unfortunately there is no experimental evidence of this behavior, e.g. recent $I(s)$ measurements on related molecular wires have found an opposite and expected trend, with the conductance increasing as the contact gap is reduced. [12, 13]. Despite the apparent disagreement between the theoretically predicted phenomenon and the experimental observations, it is worth investigating further the causes for this unusual effect. If well understood, it might be

14

exploited in an actual device. A previous study [41] on a PDT wire, in which the junction was stretched asymmetrically, looked into the density of states (DOS) and observed a better alignment between the HOMO and gold Fermi level, which more than compensates for the reduced coupling to the electrodes. A close correspondence between the frontier orbitals and associated energies of the phenylthiolate radical adsorbed on the gold surface and those of the isolated phenylthiol was demonstrated before [26]. Hence, for the sake of comparison with the current transport work it is more appropriate to investigate the effect of the symmetric removal of the two hydrogen atoms from the thiol groups of the isolated PDT [36]. One then finds that in the dehydrogenated form the original HOMO, a highly conjugated $\pi$ state which extends across the backbone, is emptied and becomes the LUMO of the PDT biradical. The zero-bias transmission spectra in Fig. 5 demonstrate a very similar effect when the separation of OPV3 from the contacts is increased. At the equilibrium junction geometry (the fifth panel from the top) the flat broad peak below the Fermi energy arises mostly from the contributions from the three electronic states with strong hybridization between gold and sulfur orbitals [26]. With increasing the separation the interaction with gold electronic states weakens and the broad structure evolves into discrete resonances (the fourth, third, and second panel in Fig. 5) while the molecule adopts again a more biradical character. Two peaks in particular, with principal contributions from HOMO-1 and HOMO, begin to emerge and rise in energy as the distance from the leads increases. Eventually, at the extra separation of 3.5 Å, all the peaks in the transmission spectrum (top panel in Fig. 5) arise simply from the molecular electronic states, as the contributions to the DOS from one of the S atoms, also shown in the upper panel of Fig. 5 indicate. A comparison of the frontier molecular orbitals of the isolated biradical with their counterparts in the 3.5 Å stretched junction is presented in Fig. 7. The removal of the H atoms from the thiol groups

15

results in a new doubly degenerate HOMO of the biradical, with largest weights on the two S atoms as an in-plane $\pi$ orbital. In the stretched junction this contribution to the DOS, shown as the red peak in the top panel of Fig. 5, coincides with the Fermi level of the leads, with the HOMO-1 peak only slightly below it. The nearly perfect match in energy of the highest occupied states in the leads and wire, and the notable spatial extent of the HOMO in the direction of the leads, results in a significant coupling strength with contacts, in spite of the distance. The coupling is manifested by the substantial weight of the hybrid of the HOMO with the Fermi level of gold on the surface atoms, shown in Fig. 7. The weight of the HOMO-1 on the leads appears even more prominent than that of the HOMO, implying a more bonding character of the lower lying state, albeit less directional and less overlapping with gold. Hence, despite the large gap elongation of 3.5 Å, the S-S distance is also notably extended, by 0.34 Å (Table I), relative to the value in the free OPV3, reflecting a substantial attractive interaction at the interfaces.

In addition to the band alignment and coupling strength, in the NEGF formalism a high conductance also requires a substantial orbital overlap across the junction. The HOMO is rather localized at the wire ends and, as such, it cannot contribute substantially to the charge transport. However, the two closest orbitals, HOMO-1 and LUMO, shown in Fig. 7, happen to be conjugated $\pi$ states with a high degree of overlap over the whole carbon backbone. They manifest in the DOS in Fig. 5 as the left and right shoulder peaks to the dominant HOMO contribution. The LUMO corresponds to the HOMO of the OPV3 before the removal of the H atoms (shown in Fig. 8), as predicted for PDT [36]. As a consequence of these two DOS contributions, the corresponding transmission coefficient, shown in the top panel of Fig. 5, exhibits two narrow, sharp peaks just below and above the Fermi level. Hence, the OPV3 wire in a stretched gold junction is characterized by the

16

extremely favorable band alignment of the three most important biradical orbitals with the Fermi level, a moderate electronic coupling of the latter with the HOMO, and the highly conjugated nature of the other two orbitals. The interplay between these contributions gives rise to the unusually large zero-bias conductance.

The application of bias, $V_b$, across the junction produces a relative shift between the quasi-Fermi levels of the left and right leads, $\mu_L$ and $\mu_R$, respectively, of $\mu_L - \mu_R = eV_b$. Therefore the bias is expected to lift the degeneracy of the HOMO of the OPV3 wire in the stretched junction with the Fermi levels of the gold leads and weaken their hybridization. Consequently, this should result in a reduced conductance. However, in the case of OPV3 in the stretched junction, the finite bias transmission spectra $T(E, V_b)$ (shown in Fig. 6) exhibit little variation with the bias $V_b$. In a bias range of $(-0.5, 0.5)$ V the two peaks around $E = 0$, now relative to the average of the electrochemical potentials $(\mu_L + \mu_R)/2$, remain qualitatively the same as those of the zero bias spectrum in the top panel of Fig. 5. This demonstrates that, under the low voltage gradients across the stretched junction, the HOMO-1 and LUMO are not affected by the lead potentials and their energies are floating independent of the bias. Only for a bias outside this range the two peaks begin to shift toward lower and higher energies, respectively, as the bottom panel of Fig. 6 shows. This suggests that, under the increased voltage gradients across the junction, the HOMO-1(LUMO) becomes pinned to the electrode with the lower (higher) electrochemical potential. As the energy gap between the levels widens, the transmission amplitude in the middle sharply drops. Consequently, the I-V characteristic in the upper panel of Fig. 2 exhibits a sudden breakdown of the high conductivity for a bias $V_b > |0.5|$ V. Nevertheless, a linear I-V characteristic in a $(-0.5, 0.5)$ V bias window is predicted for this hypothetical device. This unique feature and the fact that the OPV3 wire is coupled to the contacts primarily via

the narrow HOMO resonance, which does not contribute to any transmission channel, could then be harnessed via the addition of a third, gate electrode. Electrostatic gating of the carbon backbone is expected to have little effect on the contact states, which are localized around the S caps. The potential transistor operation is provided by a combination of two essential properties [44]. On the one hand, the nature of the bonding to the leads, via the non-conducting localized HOMO, is not significantly affected by the potential on the gate terminal, while on the other, the energy positions of the two narrow conducting channels of the carbon backbone are independent of the bias over a useful voltage range. Hence, given the linear I-V characteristic in the bias window of $(-0.5, 0.5)$ V, the device could be exploited as a transistor in an amplifier circuit.

Just outside the $(-0.5, 0.5)$ V bias window, the two spectral peaks become increasingly pinned to the contacts and the small bias variations results in large current/conductance variations. Hence, in this regime the device demonstrates the potential to be utilized in a circuit as a symmetric two-terminal bias-controlled switch.

The evolution of the transmission probability through the OPV3 wire with the bias for several representative junctions is shown in Fig. 6. As discussed above, the transmission through the 3.5 Å stretched junction is almost unchanged in the $(-0.5, 0.5)$ V bias window. This is followed by a sudden drop at an increased voltage as the two peaks contributing to the conductance move apart and their magnitudes reduce. The transmission through the 1.0 Å extended junction closely follows that of the 30º tilted wire in a 2.0 Å contracted junction at low and moderate voltages, with the latter always slightly higher in the relevant bias window, though. Consequently, the calculated current is substantially higher for the tilted wire. The compressed wire in the 2.0 Å contracted junction exhibits a similar trend, though its transmission is consistently below that of the tilted wire or the wire in the extended

18

junction.

The predicted operation of the OPV3 wire in the elongated junction is very appealing and it would be interesting to test if similar behavior can be experimentally observed. Naturally, the present study only indicates the physical principles behind the action of such a junction. Since electronic structure calculations, such as DFT, cannot evaluate the band alignment with necessary accuracy [45, 46], the design of the actual device would require fine tuning in the choice of electrode materials, wire linker groups and wire itself. The key problem would then be the fabrication of the device. In almost every experiment the molecular wire is attached to one or both sides of the junction. In the elongated junction the wire does not remain in the middle of the gap, but rather attaches to one of the electrode surfaces. The application of bias is also expected to affect its position. In order to overcome this obstacle the wire would first have to be firmly gated, perhaps with several side groups, to the gate terminal. The next step would involve the fabrication of the contacts around it. Two and three-terminal devices with OPVn derivatives have been successfully fabricated [3–6], but for the proposed device to operate in the desired regime a much greater degree of control over the attachment on both sides of the junction is essential. The contacts would have to operate like a vice around the gated wire. In the first step, the vice has to close in order to remove the hydrogen atoms from the end groups (if thiol linkers are used). In a subsequent step, the vice needs to open, but in a symmetric and tunable fashion, to achieve the right magnitude of coupling with the wire at both ends. Through the mechanical action of the gate and vice their key role would be to prevent the formation of fully fledged chemical bonds between the wire and leads, which would give rise to stronger coupling at the expense of the desired band alignment. Even though none of the steps in the proposed experiment seems impossible, it would clearly be very difficult to achieve the necessary degree of control. However, it

19

will be demonstrated below that the predicted characteristics of "rigid" molecular wires in stretched junctions might have already been manifested, although indirectly.

The study of the distorted wire in a compressed junction reveals more interesting details in the structural changes than in the electronic properties. The zero bias transmission spectra for the 0.5, 2.0, and 3.5 Å contracted junctions are shown in the three bottom panels of Fig. 5. The main effect of the compression manifests in the contribution of the HOMO to the transmission, which shifts slightly closer to the Fermi level, resulting in slightly enhanced conductances, as Table I shows. Thus, as in the case of the extended junctions, the trade-off between the better band alignment and the weaker contact coupling yields the higher conductance. Actually, as Table I shows, the minimum low bias conductance is predicted for the equilibrium geometry, where the bonding at the contacts is optimal, while the relevant band alignment is the least favorable.

OPV is considered to be a rigid system which owes its good conducting properties to the highly conjugated planar structure. Hence, it is somewhat surprising that even when the structure is distorted from planar by bending and twisting the rings, as is the case with the compressed 3.5 Å junction, high conductance is still preserved. An instructive insight into this effect if provided by comparison of the HOMO of the wires in the equilibrium and compressed junction (shown in Fig. 8). The HOMOs of the free molecule in the equilibrium and distorted geometry, with H atoms restored, also shown in Fig. 8. indicate that the H-S bonds have a similar effect on the frontier orbitals as the Au-S bonds. The qualitatively unchanged shape of the HOMO from the equilibrium planar molecule to the heavily distorted wire in the junction accounts for the nearly constant conductance for a range of contracted gaps. Thus, it is not so much the conformational rigidity of OPV that accounts for the good conducting properties as much as it is the resilience of its $\pi$-conjugated system. Both are

provided by the vinylene links, though. The current findings suggest that if the dominant conformational changes for a single-molecule junction arise from the bending and twisting of the wire, then for the electronically "rigid" wires, such as OPV3, the corresponding conductance is not expected to exhibit a notable conformational switching, in line with experiment [12].

The low-bias conductance of tilted OPV3 wires in contracted junctions manifests an opposing trend to that of the compressed distorted wires; namely it increases with the tilt angle (i.e. gap contraction). This effect has recently been observed experimentally by Haiss *et al* for a series of "rigid" molecular wires [12, 13], including an oligo-phenylene-ethynylene derivative with three rings (OPE3), similar to the OPV3. An explanation of this behavior is provided by the zero bias transmission spectra in Fig. 5. The sixth and the seventh panel show the spectra for the 15º and 30º OPV3 wires in the 0.5 and 2.0 Å contracted junctions, respectively, against their distorted counterparts. It is evident that contribution around the Fermi level increases with the tilt angle, as a consequence of the better band alignment. The distorted wires do not show such a clear trend. In fact the spectra of the distorted and tilted wires do not even look similar. However if, the latter are plotted against those of the elongated junctions, as in the third and the fourth panel of Fig. 5, the resemblance is remarkable. Hence, similar low bias conductances are obtained for the 0.5 and 1.0 Å stretched junctions as for the 0.5 and 2.0 Å contracted junctions, respectively, shown in Table I. While this effect might seem unusual, a closer look into the relevant geometrical parameters of the tilted wires shows it is perfectly consistent. Namely, although the gaps between the leads are contracted, the ΔS-S values in the Table I show that the tilted wires are actually elongated. In the case of the 15º tilted wire, the elongation is small, only 0.05 Å, and thus its spectrum should look more like that of the wire at the equilibrium position. Likewise,

for the 30° tilted wire the elongation is slightly below that of the 0.5 Å elongated junction, while its spectrum and the conductance is closer to that of the 1.0 Å. Clearly, the elongation of the wires is not the reason for their similar conducting properties. Rather, it is the similar nature of the electronic coupling to the electrodes that results in the similar spectra and conductance magnitudes. Because of the unfavorable bond angles between the C-S and S-Au bonds in the tilted orientation, the binding is weakened, which again yields a better band alignment. Alternatively, one can view the process of tilting the wire as that of keeping the wire upright and turning the contacts around sulphur hinges. This puts some strain on the S-Au bonds and, in turn, also on the backbone. But the key effect is the reduced binding at the interface in an approximately symmetric fashion at both ends. Originally the observed behavior was ascribed to an increased coupling strength and broader resonances [12, 13]. The present findings oppose and challenge this view. Provided that our interpretations of those measurements are correct, it would mean that the desirable conductance regime through molecular wires is achievable simply through an accurate manipulation of contact gap and wire orientation. In view of these findings, our predictions regarding the enhanced conductance of the OPV3 wire with symmetric separation from the contacts appear rather realistic.

## IV. CONCLUSIONS

The conductance of a single-molecule OPV3 wire between flat gold contacts has been modeled using the NEGF based on DFT calculations. The effects of the contact gap geometry on the conductance have been investigated. It has been predicted that a symmetrical gap elongation over a small range results in enhanced transport properties of the junction. In contrast, the contraction of the gap that results in significant molecular distortions is found to have little effect on the charge transport. Finally, the contraction of the gap that causes the wire to tilt at an angle is found to be geometrically analogous to the case of symmetrically stretched junction, with similarly improved transport properties. The latter findings confirm previous experimental observations, while providing an alternative interpretation. Given the "rigid" conjugated frontier orbitals of the wire, all the present results are interpreted in terms of the better band alignment of the non-equilibrium geometries at the expense of coupling strength with the current/voltage electrodes.

**ACKNOWLEDGMENTS**

## REFERENCES

[1] N. J. Tao, Nature Nanotechnology **1**, 173 (2006).

[2] J. H. Burroughes, D. D. C. Bradley, A. R. Brown, R. N. Marks, K. Mackay, R. H. Friend, P. L. Burns, and A. B. Holmes, Nature **347**, 539 (1990).

[3] S. Kubatkin, A. Danilov, M. Hjort, J. Cornil, J. L. Brédas, N. Stuhr-Hansen, P. Hedegård, and T. Bjørnholm, Nature **425**, 698 (2003).

[4] E. A. Osorio, K. O'Neill, M. Wegewijs, N. Stuhr-Hansen, J. Paske, T. Bjørnholm, and H. S. J. van der Zant, Nano Letters **7**, 3336 (2007).

[5] A. V. Danilov, S. Kubatkin, S. Kafanov, K. Flensberg, and T. Bjørnholm, Nano Letters **8**, 2184 (2008).

[6] A. Danilov, S. Kubatkin, S. Kafanov, P. Hedegård, N. Stuhr-Hansen, K. Moth-Poulsen, and T. Bjørnholm, Nano Letters **8**, 1 (2008).

[7] S. M. Lindsay and M. A. Ratner, Adv. Mater. **19**, 23 (2007).

[8] C. Toher and S. Sanvito, Physical Review Letters **99**, 056801 (2007).

[9] D. Krüger, H. Fuchs, R. Roussseau, D. Marx, and M. Parrinello, Phys. Rev. Lett. **89**, 186402 (2002).

[10] M. G. Roper, M. P. Skegg, C. J. Fisher, J. J. Lee, V. R. Dhanak, D. P. Woodruff, and R. G. Jones, Chem. Phys. Lett. **389**, 87 (2004).

[11] K.-H. Müller, Phys. Rev. B **73**, 045403 (2006).

[12] W. Haiss, C. Wang, I. Grace, A. S. Batsanov, D. J. Schiffrin, S. J. Higgins, M. R. Bryce, C. J. Lambert, and R. J. Nichols, Nature Materials **5**, 995 (2006).

[13] W. Haiss, C. Wang, R. Jitchatia, I. Grace, S. Martín, A. S. Batsanov, S. J. Higgins, M. R. Bryce, C. J. Lambert, P. S. Jensen, et al., J. Phys. Condens. Matter **20**, 374119 (2008).

[14] D. Sánchez-Portal, P. Ordejón, E. Artacho, and J. M. Soler, International Journal of Quantum Chemistry **65**, 453 (1997).

[15] J. M. Soler, E. Artacho, J. D. Gale, A. García, J. Junquera, P. Ordejón, and D. Sánchez-Portal, Journal of Physics: Condensed Matter **14**, 2745 (2002).

[16] L. Kleinman and D. M. Bylander, Physical Review Letters **48**, 1425 (1982).

[17]  N. Troullier and J. L. Martins, Physical Review B **43**, 1993 (1991).

[18]  J. P. Perdew, K. Burke, and M. Ernzerhof, Physical Review Letters **77**, 3865 (1996).

[19]  O. F. Sankey and D. J. Niklewski, Physical Review B **40**, 3979 (1989).

[20]  J. Junquera, Ó. Paz, D. Sánchez-Portal, and E. Artacho, Physical Review B **64**, 235111 (2001).

[21]  R. C. Hoft, M. J. Ford, and M. B. Cortie, Molecular Simulations **33**, 897 (2007).

[22]  M. J. Ford, R. C. Hoft, A. M. McDonagh, and M. B. Cortie, Journal of Physics: Condensed Matter **20**, 374106 (2008).

[23]  A. R. Rocha, V. M. Garcia-Suarez, S. W. Bailey, C. J. Lambert, J. Ferrer, and S. Sanvito, Nature Materials **4**, 335 (2005).

[24]  A. R. Rocha, V. M. Garcia-Suarez, S. W. Bailey, C. J. Lambert, J. Ferrer, and S. Sanvito, Physical Review B **73**, 085414 (2006).

[25]  I. Rungger and S. Sanvito, Physical Review B **78**, 035407 (2008).

[26]  A. Bilić, J. R. Reimers, and N. S. Hush, J. Chem. Phys. **122**, 094708 (2005).

[27]  A. Bilić, J. R. Reimers, N. S. Hush, and J. Hafner, J. Chem. Phys. **116**, 8981 (2002).

[28]  A. Bilić, J. R. Reimers, and N. S. Hush, J. Phys. Chem. B **106**, 6740 (2002).

[29]  J. Zhang, A. Bilić, J. R. Reimers, N. S. Hush, and J. Ulstrup, J. Phys. Chem. B **109**, 15355 (2005).

[30]  A. Bilić, J. R. Reimers, N. S. Hush, R. C. Hoft, and M. J. Ford, J. Chem. Theory Comput. **2**, 1093 (2006).

[31]  S. Piana and A. Bilic, J. Phys. Chem. B **110**, 23467 (2006).

[32]  P. F. Cafe, A. G. Larsen, W. Yang, A. Bilic, I. M. Blake, M. J. Crossley, J. Zhang, H. Wackerbarth, J. Ulstrup, and J. R. Reimers, J. Phys. Chem. C **111**, 17285 (2007).

[33]  J. R. Reimers, G. C. Solomon, A. Gagliardi, A. Bilić, N. S. Hush, T. Frauenheim, A. D. Carlo, and A. Pecchia, J. Phys. Chem. A **111**, 5692 (2007).

[34]  M. Hasan, D. Bethell, and M. Brust, J. Am. Chem. Soc. **124**, 1132 (2002).

[35]  Ž. Crljen, A. Grigoriev, G. Wendin, and K. Stokbro, Physical Review B **71**, 165316 (2005).

[36]  L. Romaner, G. Heimel, M. Gruber, J. L. Brédas, and E. Zojer, Small **2**, 1468 (2006).

[37]  R. C. Hoft, M. J. Ford, V. M. Garcia-Suarez, C. J. Lambert, and M. B. Cortie, Journal of Physics: Condensed Matter **20**, 025207 (2008).

[38]  B. Q. Xu and N. J. Tao, Science **301**, 1221 (2006).

[39]  S. Datta, W. Tian, S. Hong, R. Reifenberger, J. I. Henderson, and C. P. Kubiak, Phys. Rev.

Lett. **79**, 2530 (1997).

[40] P. S. Damle, A. W. Ghosh, and S. Datta, in *Molecular Electronics*, edited by M. A. Reed and T. Lee (American Scientific Publishers, 2003), p. 115.

[41] Y. Xue and M. A. Ratner, Phys. Rev. B **68**, 115407 (2003).

[42] V. M. García-Suárez, T. K. S. Bailey, C. Lambert, and B. R. Bulka, Phys. Stat. Sol. B **244**, 2443 (2007).

[43] C. Toher and S. Sanvito, Physical Review B **77**, 155402 (2008).

[44] A. Grigoriev, J. Sköldberg, G. Wendin, and Ž. Crljen, Physical Review B **74**, 045401 (2006).

[45] Y. Xue, S. Datta, and M. A. Ratner, J. Chem. Phys. **115**, 4292 (2001).

[46] J. R. Reimers, Z. L. Cai, A. Bilić, and N. S. Hush, Ann. N.Y. Acad. Sci **1006**, 235 (2003).

[47] S. D. Fleming and A. L. Rohl, Zeitschrift für Kristallographie **220**, 580 (2005).

[48] A. Kokalj, Comp. Matter. Sci. **28**, 155 (2003).

TABLE I: Low bias conductance, $\sigma$, of the OPV3 wire for the considered junction geometries. $\Delta$S-S is the difference in the separation between two S atoms relative to the distance of 19.63 Å for an isolated biradical.

| gap separation [Å] | $\Delta$S-S [Å] | $\sigma[\mu$S] |
|---|---|---|
| +3.5 | +0.34 | 15.60 |
| +1.5 | +0.64 | 5.30 |
| +1.0 | +0.45 | 3.73 |
| +0.5 | +0.25 | 2.87 |
| equilibrium | +0.03 | 2.40 |
| -0.5 | -0.43 | 2.56 |
| -1.0 | -1.20 | – |
| -2.0 | -2.32 | 2.55 |
| -3.5 | -3.93 | 2.57 |
| -0.5, 15° tilted | +0.05 | 2.88 |
| -2.0, 30° tilted | +0.20 | 3.87 |

FIG. 1: The two isomers of OPV3

FIG. 2: Upper panel: current vs. bias voltage for the junctions symmetrically stretched away from the equilibrium geometry. Lower panel: current vs. bias voltage for the junctions contracted starting from the equilibrium geometry.

FIG. 3: The effect of gradual compression, in steps of 0.5 Å, on the OPV3 wire, starting from the equilibrium geometry. Graphic produced with GDIS [47] program.

FIG. 4: The orientation of the OPV3 wire in the (a) 0.5 and (b) 2.0 Å contracted junction tilted at an angle of 15º and 30º, respectively. Graphic produced with GDIS [47] program.

FIG. 5: The zero-voltage transmission through the OPV3 wire in extended (four top panels) and compressed (three bottom panels) states. The fifth panel shows the transmission probability at the equilibrium junction geometry. The top panel also shows the contributions to the projected density of states (DOS) on one of the S atoms for the 3.5 Å elongated junction. The green dashed line shows the transmission coefficient for the the OPV3 wire in the 0.5 and 2.0 Å contracted junction tilted at an angle of 15º (panels four and six) and 30º (panels three and seven), respectively. The energy is given relative to the Fermi level, $E_F$.
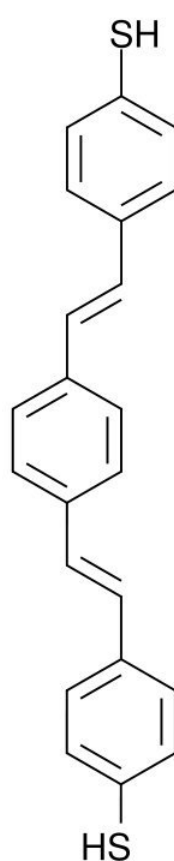
FIG. 6: The transmission probability through the OPV3 wire in the 3.5 Å and 1.0 Å extended and 2.0 Å compressed junctions. The top panel shows the transmission at the zero bias, the middle panel at a bias voltage of 0.4 V, and the bottom panel at a bias voltage of 0.8 V. The vertical lines mark the bias window.

FIG. 7: The shape of the frontier orbitals (doubly degenerate HOMO) of OPV3 in the 3.5 Å extended junction and in the isolated biradical. Graphic produced with XCrySDen [48] package.
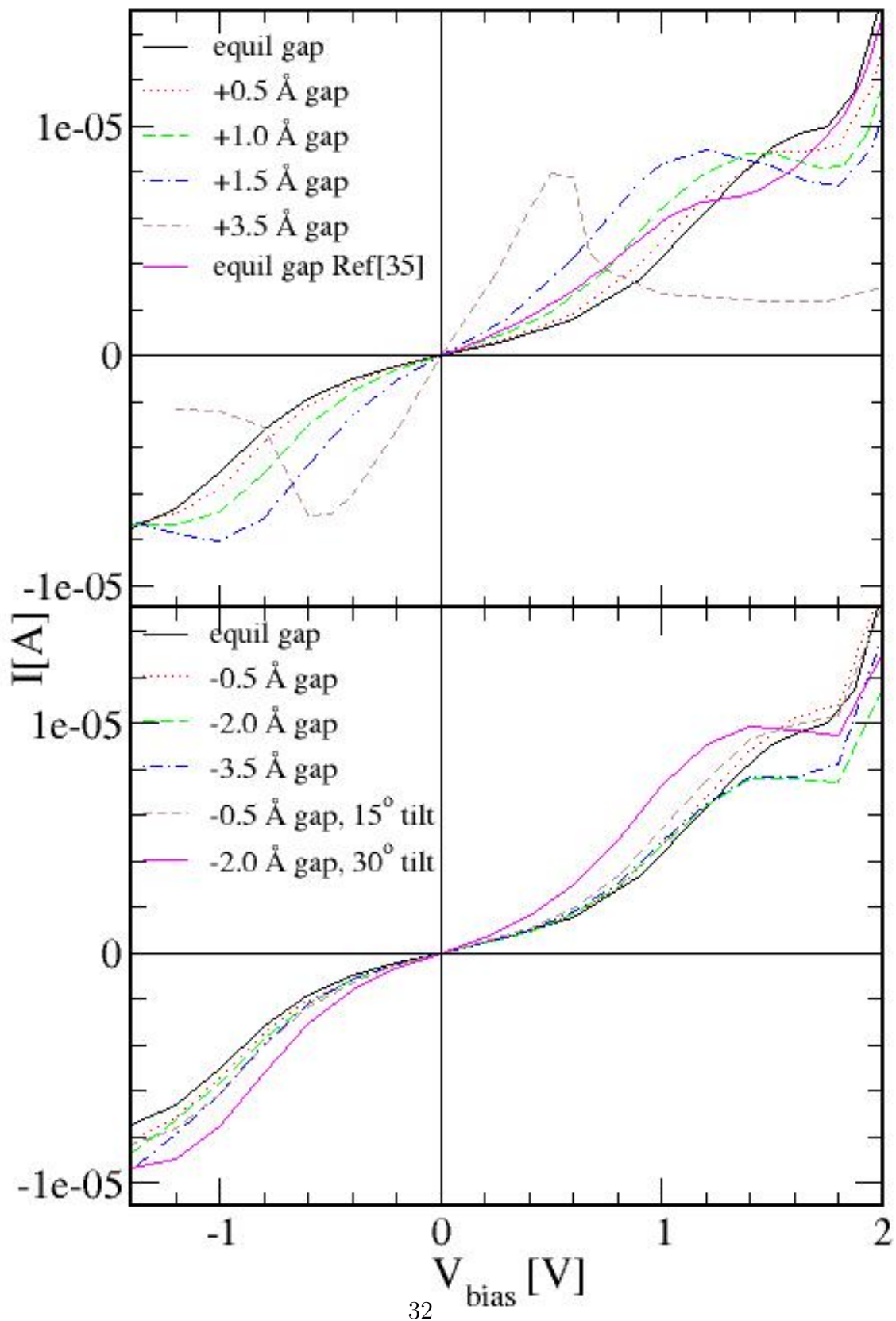
FIG. 8: Top: the shape of the HOMO of OPV3 in the equilibrium and 3.5 Å extended junction. Bottom: the HOMO of the isolated OPV3 molecule in the same backbone geometry (hydrogen atoms restored), Graphic produced with XCrySDen [48] package.
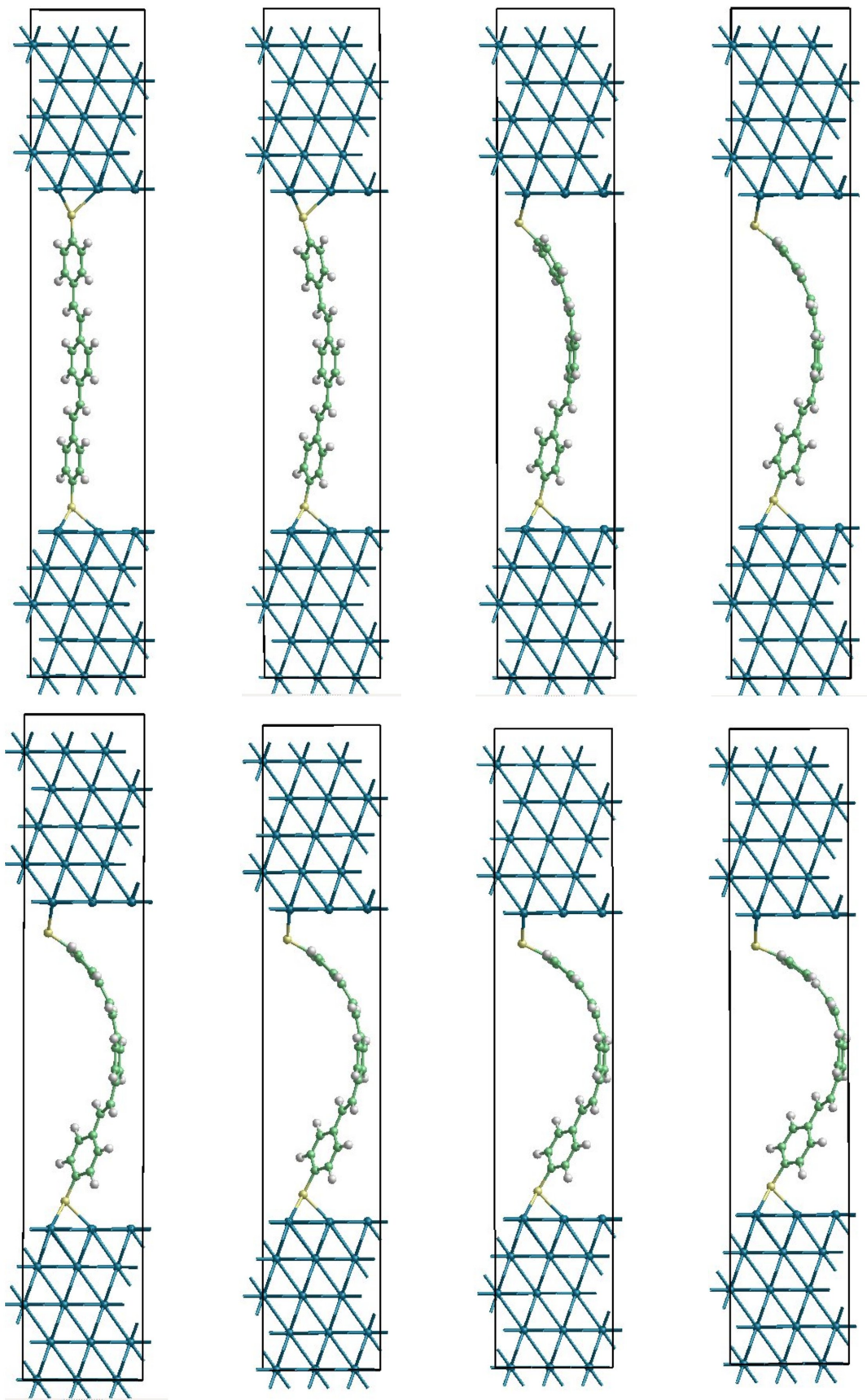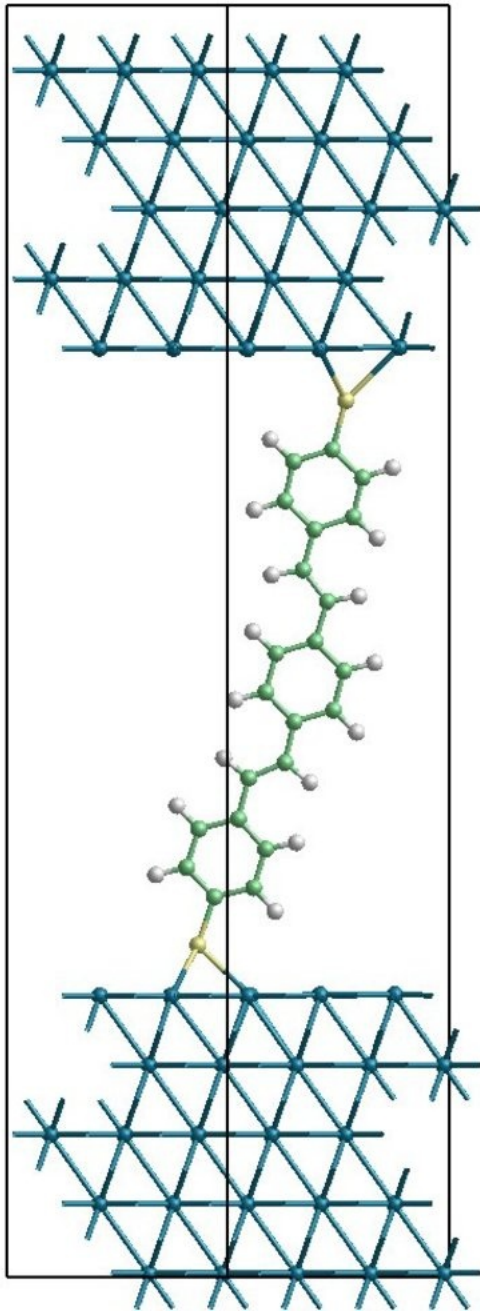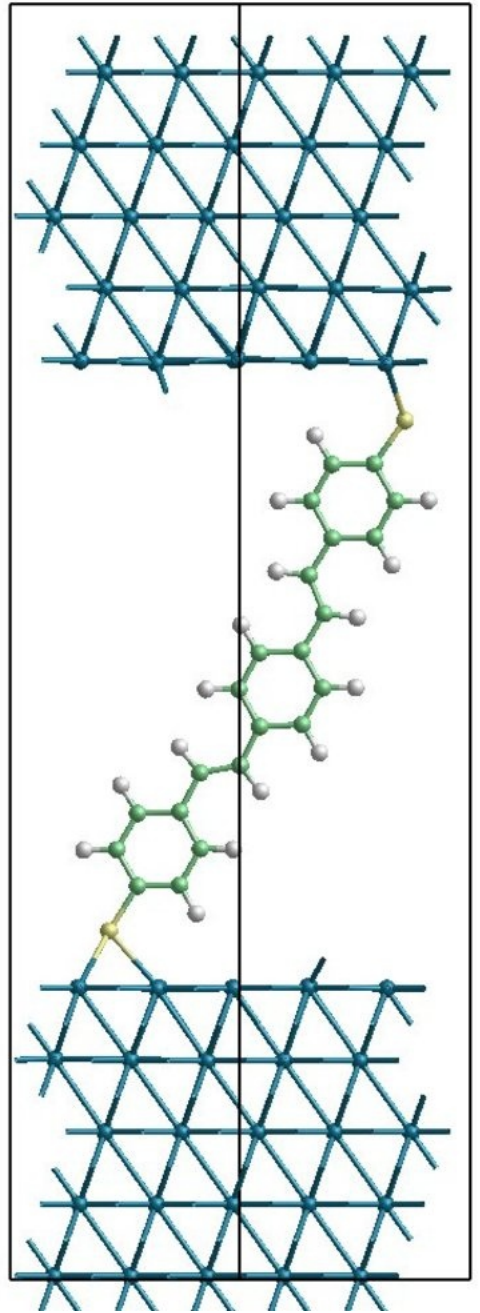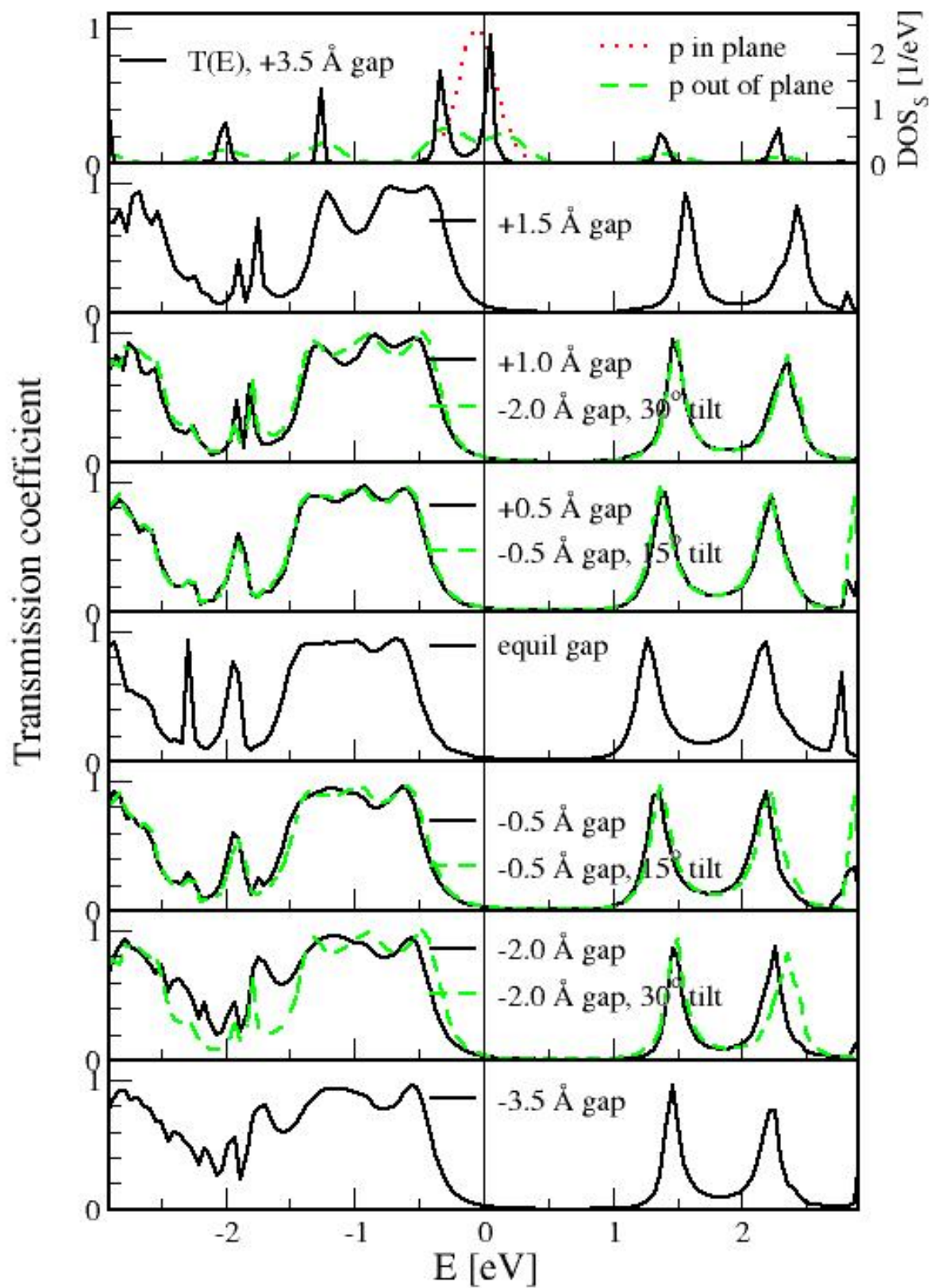
trans,trans          trans,cis

Figure axes: vertical axis labeled "Transmission coefficient" (left) and "DOS$_S$ [1/eV]" (right); horizontal axis labeled "E [eV]".

Panel labels (top to bottom): T(E), +3.5 Å gap; p in plane; p out of plane; +1.5 Å gap; +1.0 Å gap, -2.0 Å gap, 30° tilt; +0.5 Å gap, -0.5 Å gap, 15° tilt; equil gap; -0.5 Å gap, -0.5 Å gap, 15° tilt; -2.0 Å gap, -2.0 Å gap, 30° tilt; -3.5 Å gap.
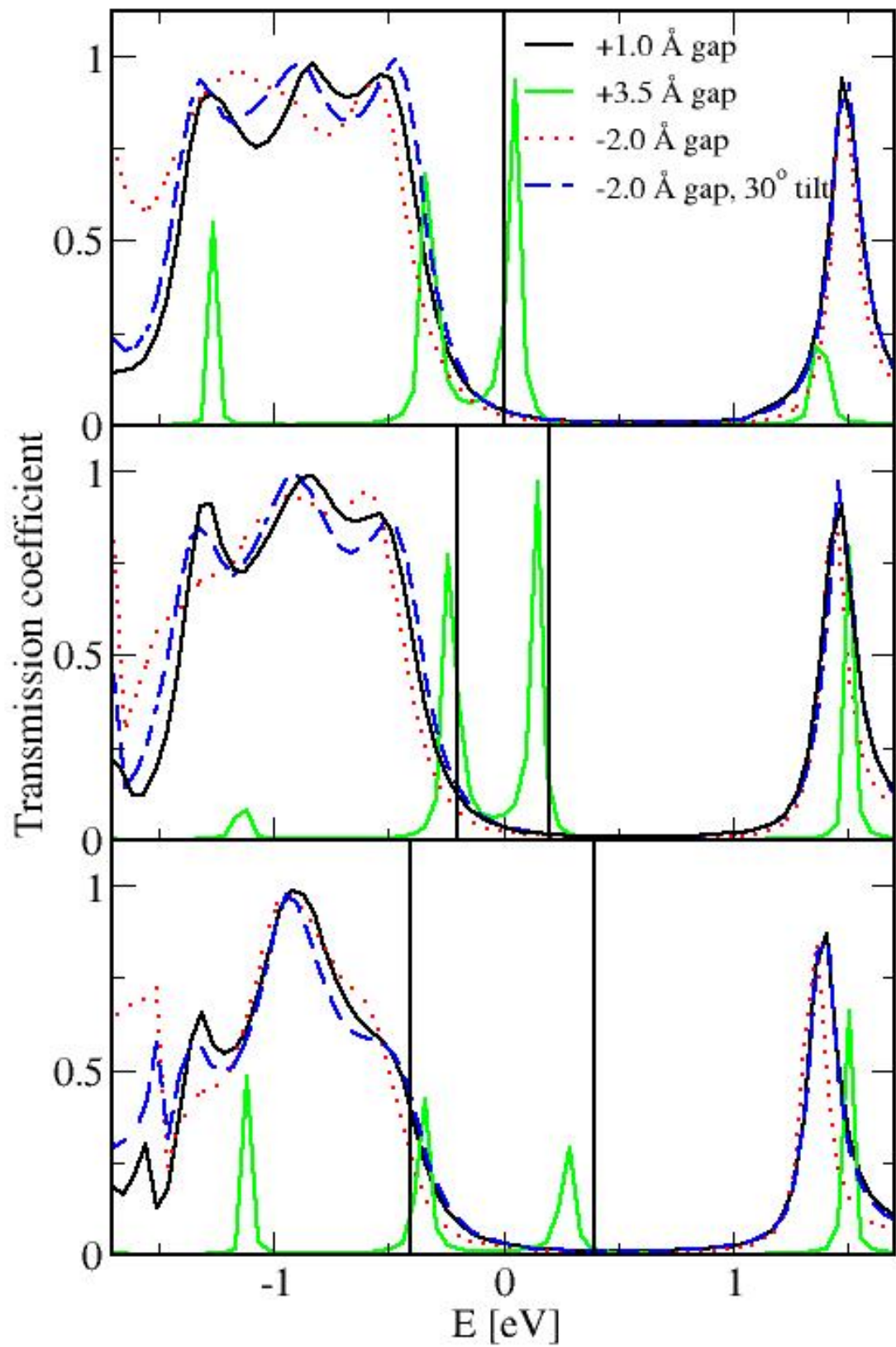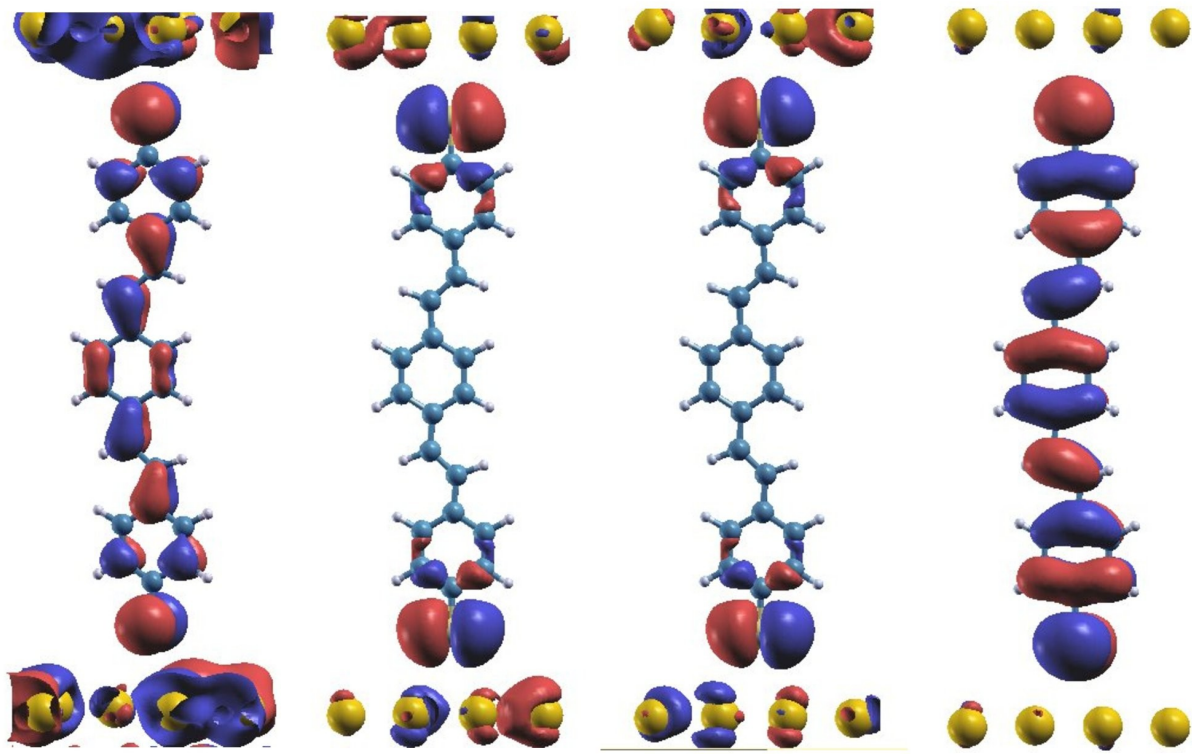
HOMO-1          HOMO'          HOMO''          LUMO